

Discussion and Visualization of Distinguished Hyperbolic Trajectories as a Generalization of Critical Points to 2D Time-dependent Flow

Roxana Bujack*

Los Alamos National Laboratory

ABSTRACT

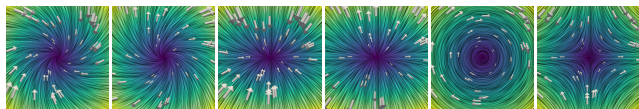
Classical vector field topology has proven a useful visualization technique for steady flow, but its straightforward application to time-dependent flows lacks physical meaning. Necessary requirements for physical meaningfulness include the results to be objective, i.e., independent of the frame of reference of the observer, and Lagrangian, i.e., that the generalized critical points are trajectories. We analyze whether the theoretical concept of distinguished hyperbolic trajectories provides a physically meaningful generalization to classical critical points and if the existing extraction algorithms correctly compute what has been defined mathematically. We show that both theory and algorithms constitute a significant improvement over previous methods.

We further present a method to visualize a time-dependent flow field in the reference frames of distinguished trajectories. The result is easy to interpret because it makes these trajectories look like classical critical points for each instance in time, but it is meaningful because it is Lagrangian and objective.

Keywords: visualization, vector field, flow, topology, Lagrangian, objective, time-dependent, distinguished hyperbolic trajectory

1 INTRODUCTION

Vector field topology has become a popular methodology for the visualization of flow fields. For steady flows, it is able to extract relevant information from the data, which can be used for semantically meaningful compression and to reduce occlusion in visualizations.



(a) S. sink: $\Re(\lambda_i) < 0$, $\Im(\lambda_i) \neq 0$. (b) S. src: $\Re(\lambda_i) > 0$, $\Im(\lambda_i) \neq 0$. (c) N. sink: $\Re(\lambda_i) < 0$, $\Im(\lambda_i) = 0$. (d) N. src: $\Re(\lambda_i) > 0$, $\Im(\lambda_i) = 0$. (e) Center: $\Re(\lambda_i) = 0$, $\Im(\lambda_i) \neq 0$. (f) Saddle: $\Re(\lambda_1) > 0$, $\Re(\lambda_2) < 0$, $\Im(\lambda_i) = 0$.

Figure 1: Types of critical points classified by the eigenvalues of the Jacobian visualized via arrow glyphs and line integral convolution (LIC) [8]. Color represents speed: blue (low), yellow (high).

The **topological skeleton** segments the domain into areas of coherent flow behavior. It comprises **critical points**¹, which are locations where the vector field is zero, and **separatrices**, which are the codimension-one invariant manifolds. Figure 1 illustrates how critical points are categorized into saddles, sinks sources, and centers depending on the eigenvalues of their Jacobian, i.e., their velocity gradient.

*e-mail: bujack@lanl.gov

¹Critical points are the most common name in the context of vector field topology, but mathematically less ambiguous names are singularities, stationary points, equilibria, or zero points.

Application of the classical (steady) vector field topology to each instance in time works well for the analysis of electric and magnetic fields, but this approach loses physical meaning for time-dependent (unsteady) flow fields. Flow visualization researchers have investigated generalizations of the classical vector field topology that preserves physical meaning but provides an intuitive visualization similar to its classical counterpart. But physical meaning cannot be defined mathematically. What can be formulated mathematically are requirements that have to be fulfilled, to assign physical meaning to observed structures. A second challenge in a time-dependent setting is that time-varying data is usually only provided on a finite time interval, while certain theoretical concepts that are used in the steady theory of dynamical systems, like hyperbolicity or convergence, are only defined asymptotically for an infinite temporal domain.

Physical meaningfulness. Mathematical concepts that are frequently used in the literature as examples of why the classical vector field topology is not physically meaningful have been collected by Bujack et al. [7]. **Objectivity** is one of them. It refers to the concept that extracted features do not change under a Euclidean change of the reference frame. Another popular criterion considered necessary to ensure physical meaning is **Lagrangian invariance**. A feature is Lagrangian if it develops over time as if it were advected by the flow, like pathlines or material surfaces. **Generalization.** We call a method a true generalization of the classical vector field topology if it **coincides with classical vector field topology** for steady input fields. That means if the input field is given as a time series that happens to be constant over time, then extracted features must be the classical critical points and separatrices.

A general observation is that there is currently no available algorithm that is Lagrangian, objective, and coincides with the classical vector field topology on steady fields.

Distinguished hyperbolic trajectories (DHTs) [22] arise from the theory of dynamical systems and are a promising concept for the generalization of critical points. Here a trajectory is called **hyperbolic** if the corresponding linearization of the flow has a full set of exponentially growing or decaying solutions and **distinguished** if it remains in a bounded neighborhood for all time while all its neighbors leave this neighborhood.

Contributions. We analyze the properties of distinguished hyperbolic trajectories to find out to what extent they can generalize the classical vector field topology in a physically meaningful way. Specifically, we provide theorems and counterexamples to show if they are Lagrangian, objective, and if they coincide with classical critical points if the input vector field happens to be steady. We extend this analysis to existing algorithms for their detection, and demonstrate that they are superior to previous approaches. Further, we suggest a method to visualize distinguished trajectories in a manner that most intuitively uses the visual language of the the classical vector field topology. In a nutshell, our contributions answer the following two questions.

- To what extent do distinguished hyperbolic trajectories generalize the critical points from classical vector field topology in a physically meaningful way?
- How can DHTs be visualized to most intuitively resemble classical critical points in a physically meaningful way?

2 RELATED WORK

We will first treat related work from flow visualization that is targeted at generalizing classical vector field topology to the time-dependent setting [18, 26, 27, 33, 46] and summarize to what extent these methods satisfy the three desirable properties: Lagrangianity, objectivity, and coincidence with the classical case. The proofs for these statements can be found in a recent state of the art report [7]. We then review work on distinguished hyperbolic trajectories.

2.1 Tracking of Steady Topology

The first application of vector field topology to unsteady flow naturally tracks topological features over time. The challenges lie in the correct association of features from one time step to another and in identifying events that change the topology, such as merges, splits, births, and deaths of critical points.

Helman and Hesselink [19, 20] introduced vector field topology to the visualization community and provided the first algorithm for tracking over time. They compute critical points for each time step, and connect them graphically.

Later tracking algorithms made use of spacetime representations assuming linear interpolation between two consecutive time steps [12, 42, 43, 50]. This allows to compute the paths of critical points by analytically solving a system of equations and makes it sufficient to analyze the cell faces to detect topological changes.

A different group of approaches [39–41, 47] leverages Feature Flow Fields that allow derivation of the paths of critical points in a d -dimensional time-dependent vector field through integration in a $(d + 1)$ -dimensional steady field. This technique can be utilized to track other topological features and vortices.

All these methods share identical mathematical properties. They coincide with the classical vector field topology, but are neither Lagrangian nor objective.

2.2 Flow Steadification

Hadwiger et al. [15] solve a global optimization problem over space and time to find an observer field that allows us to perceive the flow “as steady as possible” while maintaining the largest possible similarity between neighboring observers.

Rojo et al. [35] extract steady topology using a local frame of reference adaptation similar to Günther et al. [14]. For each point in space and time, they find the coordinate transform that minimizes the temporal derivative of the flow in its spatial neighborhood. A Taylor approximation of the transformation allows them to solve this problem using a least-squares approach. Based on the transformation they get a decomposition of the flow into its steadified part and the part that describes how this steady part moves.

Both approaches are objective and coincide with the steady case in principle, but are not Lagrangian.

2.3 Categorize or Cluster Pathlines

In a steady flow field, trajectories and streamlines coincide. However, in unsteady flow fields, they do not, and trajectories are Lagrangian, unlike streamlines. This motivates researchers to categorize or cluster pathlines to develop a physically meaningful time-dependent flow topology.

Theisel et al. [41] segment the domain into areas of convergent behavior, divergent behavior, or neither by projecting the flow on planes orthogonal to pathlines in spacetime.

One group of methods in this category [5, 28, 36, 44] uses the intersections of ridges in the forward and backward *finite-time Lyapunov exponent field (FTLE)* [17]. This generalizes saddle-type critical points to time-dependent vector fields as it ensures both expanding and contracting behavior forward as well as backward in time in accordance with the definition of hyperbolic trajectories by Haller [16]. Generalized streaklines [49] started at these intersections form a generalization of separatrices to time-dependent flows.

Wiebel et al. [48] generalize the concept of sinks by following particles that were seeded uniformly across space and time. At any given time, they compute the density of the locations where these particles were advected to and track the local maxima of this scalar field. This was the first method that was able to capture the flow structure in a rotating Petri-dish dataset.

Bujack et al. [4] derive a unified framework based on the finite time expansion and contraction of the flowmap spanning saddle-, source-, and sink-type regions.

Most of these methods are objective, but do not coincide with the steady case. Even though they are pathline-based, many approaches are not Lagrangian because they use a sliding window approach.

2.4 Generalization of Critical Points

A large group of approaches makes use of derived scalar fields and utilizes their extrema or zeros to define generalized critical points, e.g., the acceleration magnitude [11, 24, 25, 28, 34], Jacobian [6] [45], or generalized robustness [45].

Fuchs et al. [11] further suggest selecting pathlines that observe an almost steady flow in their neighborhood and have a small acceleration magnitude as generalized critical points.

The majority of the chosen scalar characteristics are Galilean invariant, but not objective. The zeros of the acceleration coincide with the classical critical points. The other methods do not. The methods are in general not Lagrangian, but Lagrangian smoothing has been suggested [11, 24], which would make a method Lagrangian if the smoothing is used as a complete averaging over the whole integration time [13]. The method by Machado et al. [28] deserves specific attention, because it suggests an iterative algorithm approximating a pathline close to a zero acceleration magnitude line, which makes it Lagrangian if it converges.

2.5 Distinguished Hyperbolic Trajectories

Ide et al. [22] analyze distinguished hyperbolic trajectories. They generalize hyperbolicity to a finite-time setting and show how to derive a coordinate transformation based on a Eulerian structure, like a critical point, that makes the linearization around it steady and diagonal so that exponential dichotomies can be detected. A real-world application was provided by Mancho et al. [29].

Ju et al. [23] improve the work by Ide suggesting an iterative algorithm starting at the critical points. It can be shown to converge toward DHTs under certain conditions. This iteration no longer requires neglecting the non-linear part of the forcing during the localization step. Ju et al. also provide conditions for the existence and uniqueness of DHTs. Later Branicki and Wiggins [2] applied the iterative algorithm to extract 2D invariant manifolds in 3D autonomous flow with focus on mesh refinement and regularization. Since extracting DHTs is difficult, the opposite approach, i.e., detecting invariant manifolds heuristically first and deriving the locations of the DHTs from them, is also discussed [3, 30].

The iterative algorithm by Ju et al. [23] does not always converge and the quality of the result depends on the quality of the initial guess. Hofmann and Sadlo [21] improve the initial estimate for saddle type DHTs making use of steadified reference frames.

3 BACKGROUND ON DHTs

In this section, we will provide the background on distinguished hyperbolic trajectories (DHTs) following the notation of Ide [22]. We will focus on the aspects that are necessary for Section 4 to analyze to what extent DHTs can generalize vector field topology to a time-dependent setting. We will see that there is a difference between the theoretical definition of a DHT and what the detection algorithms extract.

3.1 Definition

The definition of DHTs relies on linearizations, hyperbolicity, and exponential dichotomies.

3.1.1 Hyperbolicity

Let $u : \mathbb{R}^2 \times \mathbb{R} \rightarrow \mathbb{R}^2$ be 2-dimensional velocity field

$$\dot{z} = u(z, t) \quad (1)$$

and

$$\dot{\xi} = \nabla u(z(t), t)\xi \quad (2)$$

its **linearization** around a trajectory $z(t) : \mathbb{R} \rightarrow \mathbb{R}^2$ with the Jacobian $\nabla u : \mathbb{R} \times \mathbb{R}^2 \rightarrow \mathbb{R}^{2 \times 2}$. An **exponential dichotomy** [10] is a generalization of classical hyperbolicity to finite time settings defined as follows. Equation (2) has an exponential dichotomy for the finite time interval $[t_0, t_1] \subset \mathbb{R}$ if there exists a projection $P : \mathbb{R}^2 \rightarrow \mathbb{R}^2$ and positive constants $K, L, \alpha, \beta \in \mathbb{R}$ such that its fundamental matrix $X(t, t_0) : \mathbb{R} \times \mathbb{R} \rightarrow \mathbb{R}^{2 \times 2}$, i.e., the matrix-valued function whose columns are linearly independent solutions of the system [9], satisfies

$$\begin{aligned} |X(t, t_0)PX^{-1}(s, t_0)| &\leq Ke^{-\alpha(t-s)} \text{ for } t \geq s, \\ |X(t, t_0)(Id - P)X^{-1}(s, t_0)| &\leq Le^{-\beta(t-s)} \text{ for } t \leq s \end{aligned} \quad (3)$$

for all $t, s \in [t_0, t_1]$.

Ide calls a trajectory $z(t)$ of u **hyperbolic** if its linearization has an exponential dichotomy [22]. They show that there exists a time-dependent linear coordinate transform that transforms equation (2) into a system of ordinary differential equations with constant diagonal matrix and that the property of having an exponential dichotomy is frame independent. They further state that for constant matrices $\nabla u \in \mathbb{R}^{2 \times 2}$, a trajectory has an exponential dichotomy iff none of its eigenvalues has a vanishing real part. Therefore we can consider a trajectory hyperbolic if its localized and steadified Jacobian has only eigenvalues with non-zero real parts [31, 32].

3.1.2 Distinguished Hyperbolic Trajectory (DHT)

For a velocity field of the form

$$\dot{y} = Dy + g(y, t) \quad (4)$$

with constant linear part $D \in \mathbb{R}^{2 \times 2}$ and non-linear part $g : \mathbb{R} \times \mathbb{R}^2 \rightarrow \mathbb{R}^2$, let $y(t) : \mathbb{R} \rightarrow \mathbb{R}^2$ be a trajectory that remains in a bounded domain for all time, then it is a **distinguished hyperbolic trajectory (DHT)** if it is hyperbolic and there exists a neighborhood $B \subset \mathbb{R}^2$, in which $y(t)$ remains for all times while all other trajectories leave it. Further, Ide et al. require $y(t)$ to not be contained in the invariant set of another hyperbolic trajectory. An illustration can be found in Hofmann and Sadlo, Fig. 6 [21]. Note that we will leave the last constraint out of our analysis in this paper. Since the property of a point to be critical is purely local, while the property of a trajectory to be in the chaotic invariant set of another is not, the two concepts would be different in a trivial way if this criterion would be applied.

For a velocity field of the form (1), distinguished hyperbolic trajectories can be defined if there exists a coordinate transform $y = A(t)x + b(t)$ based on the movement of a Eulerian structure that transforms equation (1) into equation (4) that does not produce exponential growth or decay in the inhomogeneous part g . Then $x(t)$ is a DHT of equation (1) iff $y(t) = A(t)x + b(t)$ is a DHT of equation (4) [22].

3.2 Detection

We will first describe the algorithm for the detection of distinguished hyperbolic trajectories as suggested by Ide et al. [22] and then look at the iterative extension by Ju et al. [23]. We will follow the notation by Ide et al. [22], which results in the series of coordinate

transformations going the non-alphabetical route from z to x to y . Ide et al. do an excellent job illustrating the concept and extraction of DHTs through seven examples that gradually increase in complexity. We highly recommend studying them for an intuitive explanation of the concept.

3.2.1 Overview

Bottom up, DHTs are detected through these three steps:

- For a linear system with time-independent diagonal matrix $\dot{y} = Dy + g(t)$, the DHT can be computed analytically.
- A linear system with time-dependent matrix $\dot{x} = F(t)x + h(t)$ must be **steadified** through SVD of the fundamental matrix.
- An arbitrary system $\dot{z} = u(z, t)$ must be linearized through **localization** around a critical point.

We will provide the details of each step top down in the remainder of this section.

3.2.2 Non-linear System

Ide et al. show in Section 3 [22] how a non-linear system of the form (1) can be linearized by localization around a critical point or stagnation point z_c through the transformation

$$x = z - z_c, \quad (5)$$

which results in

$$\dot{x} \stackrel{(5),(1)}{=} u(x + z_c, t) - \dot{z}_c = \underbrace{\nabla u(z_c, t)x}_{F(t)} - \underbrace{\dot{z}_c}_{h^F(t)} + \underbrace{u(x + z_c) - \nabla u(z_c, t)x}_{h^{NL}(x, t)}. \quad (6)$$

This is the location where Ide et al. and Ju et al. follow different paths. Ide et al. neglect the non-linear part h^{NL} and work with

$$\dot{x} \approx F(t)x + h^F(t) = \nabla u(z_c, t)x - \dot{z}_c, \quad (7)$$

while Ju et al. keep both h^{NL} and the force term h^F .

3.2.3 Linear System with Time-dependent Matrix

Given a linear system

$$\dot{x} = F(t)x + h(t) \quad (8)$$

with time-dependent matrix $F : \mathbb{R} \rightarrow \mathbb{R}^{2 \times 2}$, Ide et al. show in Appendix A [22] how to find the coordinate transformation

$$y = A(t)x \quad (9)$$

with the matrix $A : \mathbb{R} \rightarrow \mathbb{R}^{2 \times 2}$ that makes the system time independent and diagonal. The transformations act on equation (8) via

$$\dot{y} \stackrel{(9),(8)}{=} \dot{A}x + A(F(t)x + h(t)) = \underbrace{(\dot{A} + AF(t))A^{-1}}_D \underbrace{Ax}_y + \underbrace{Ah(t)}_{g(t)}. \quad (10)$$

They construct A and the matrix $D \in \mathbb{R}^{2 \times 2}$ by solving

$$\dot{X} = F(t)X, \quad X(t_0) = I \quad (11)$$

for the function $X : \mathbb{R} \rightarrow \mathbb{R}^{2 \times 2}$ and using the SVD decomposed form

$$X(t) = B(t)e^{\Sigma(t)}R^T(t) \quad (12)$$

with $B, \Sigma, R : \mathbb{R} \rightarrow \mathbb{R}^{2 \times 2}$ through a Runge-Kutta method and setting

$$D := \frac{1}{t_1 - t_0} \Sigma(t_1), \quad A(t) := e^{(t-t_0)D}R^T(t_1)R(t)e^{-\Sigma(t)}B^T(t). \quad (13)$$

3.2.4 Linear System with Time-independent Diagonal Matrix
Ide et al., Section 2 [22], show that if the system has the shape

$$\dot{y} = Dy + g(t) \quad (14)$$

with constant diagonal matrix $D \in \mathbb{R}^{2 \times 2}$, then each component marked by the subscript $i = 1, \dots, d$ of the DHT $y^{DHT} : \mathbb{R} \rightarrow \mathbb{R}^d$ has the shape

$$y_i^{DHT}(t) = \begin{cases} \int_{-\infty}^t g_i(\tau) e^{D_{ii}(t-\tau)} d\tau, & D_{ii} < 0 \\ -\int_t^{\infty} g_i(\tau) e^{D_{ii}(t-\tau)} d\tau, & D_{ii} > 0. \end{cases} \quad (15)$$

3.2.5 Finite Time

Ide et al. point out that the DHT cannot be determined uniquely if the data is only given on a finite time interval $[t_0, t_1] \subsetneq \mathbb{R}$ [22]. Instead there exists a region in which the DHT can exist because that whole region remains in a neighborhood. They suggest computing an approximation to the DHT by extending the so-called **forcing function** $g(t) : [t_0, t_1] \rightarrow \mathbb{R}$ to infinity through a Fourier or power series $\tilde{g}(t) : \mathbb{R} \rightarrow \mathbb{R}$.

3.2.6 Algorithm by Ju et al.

Ju et al. do not neglect the non-linear part in equation (6) [23], but maintain the dependence of h on x and of g on y through

$$\dot{x} = F(t)x + h(x, t) \quad (16)$$

with

$$h(x, t) = h^F(t) + h^{NL}(x, t) = -\dot{z}_c + u(x + z_c) - \nabla u(z_c, t)x. \quad (17)$$

They then go over to

$$\dot{y} = Dy + g(y, t) = Dy + A(t)h(A^{-1}y, t) \quad (18)$$

analogously to Section 3.2.3 and suggest an algorithm that approximates the DHT iteratively through

$$y_i^{j+1}(t) = \begin{cases} \int_{t_0}^t g_i(y^j(\tau), \tau) e^{D_{ii}(t-\tau)} d\tau, & D_{ii} < 0 \\ -\int_t^{t_1} g_i(y^j(\tau), \tau) e^{D_{ii}(t-\tau)} d\tau, & D_{ii} > 0 \end{cases} \quad (19)$$

starting with the original stagnation point $y^0(t) = 0$. They use only the given finite time interval for the computation of the DHT and prove that under certain conditions, the solution of equation (19) approaches the DHT for growing time intervals.

3.2.7 Algorithm by Hofmann et al.

Hofmann et al. [21] use a slightly adapted version of the algorithm by Ju et al. [23]. The main difference is that they consider a variety of initial guesses. In addition to the critical points of the original field u , they use two steadification decompositions $u = w + f$, first the one that coincides with the zeros of the acceleration in accordance with Machado et al. [28], second the decomposition suggested by Rojo et al. [35]. They filter the zeros of w and only keep very strong saddles, but extend these short solutions through integration in f .

4 POWER AND LIMITATIONS OF DHTs AS GENERALIZATION OF CRITICAL POINTS

In the introduction, we described three important mathematical properties that we want a generalization of classical steady critical points to satisfy in a time-dependent setting: to be objective, Lagrangian, and truly generalize classical critical points. The question whether or not DHTs satisfy these properties is actually manifold, because we get different answers for the definition than for the algorithms as well as different results for time spanning the full range of the real numbers than for finite times.

This section contains the first contribution of this paper. We will answer these questions for the theory and each algorithm in its remainder. The summary of our results can be found in Table 1, which can be used as a table of contents to access this section non-linearly and skip parts. It provides references to the theorems and counterexamples, whose purpose is to back up the statements in the table. The proofs are in the appendix. The main reason for the difference between theory and practice for the algorithm by Ide is the dropping the non-linear part (7). The algorithms by Ju and Hofmann rely on the convergence to the correct solution starting from the initial guess (19).

4.1 Objectivity

In this subsection, we will answer the question of whether DHTs are objective, i.e., do not change under a Euclidean change of the reference frame. Explicitly, let $x^{DHT}(t) : \mathbb{R} \rightarrow \mathbb{R}^2$ be a DHT of a flow field $v(x, t)$, $x' = Q(t)x + r(t)$ be a change of coordinates with a time-dependent orthogonal matrix $Q : \mathbb{R} \rightarrow SO(d)$ and a time-dependent vector $r : \mathbb{R} \rightarrow \mathbb{R}^2$. Then the transformation of the DHT $Q(t)x^{DHT} + r(t)$ must be a DHT of the transformed field $v'(x', t) = Q(t)v(x, t) + \dot{Q}(t)x + \dot{r}(t)$.

4.1.1 Theory

Ide et al. prove the frame invariance of the DHTs in Appendix C [22] without restrictions on the time interval. That includes objectivity.

4.1.2 Algorithms by Ide et al. and Ju et al.

We will show two vector fields given for infinite times that differ only by a Galilean coordinate transform where the DHT is returned for one but not for the other. The finite-time non-objectivity follows as a consequence.

Example 1. *This example shows a case where the algorithm does not provide a solution for a vector field even though it finds the solution for a field that differs from the first one only by a Galilean coordinate transform; see Appendix Fig. 6 for illustration.*

The steady one-dimensional field

$$u(z) = z^2 + z \quad (20)$$

has the zeros $z_{c1} = 0, z_{c2} = -1$, which are hyperbolic because

$$\nabla u(z_{c1}, t) = 2z + 1|_{z=z_{c1}} = 1, \quad \nabla u(z_{c2}, t) = 2z + 1|_{z=z_{c2}} = -1. \quad (21)$$

We can see from the analytic solution of equation (20)

$$z(z_0, t) = \frac{z_0}{e^{-t}z_0 + e^{-t} - z_0}, \quad (22)$$

the critical points are the only ones without exponential behavior

$$z(z_{c1}, t) = \frac{0}{e^{-t}} = 0, \quad z(z_{c2}, t) = \frac{-1}{-e^{-t} + e^{-t} + 1} = -1 \quad (23)$$

which shows that they are the DHTs.

We show that the algorithms by Ide et al. and by Ju et al. detect them correctly explicitly for z_{c2} . The other case works analogously. Localization about the zero described in Section 3.2.2 results in $x_{c2} = 0$,

$$\dot{x} = F(t)x + g(x, t) \quad (24)$$

with the Jacobian $F(t) = \nabla u(z_{c2}, t) = -1$ and the forcing

$$g(x) = h(x, t) = -\dot{z}_c + u(x + z_c) - \nabla u(z_{c2}, t)x = (x - 1)^2 + x - 1 + x \quad (25)$$

being time-independent. Since $g(x_{c2}) = g(0) = 0$, it is returned as the DHT for both algorithms from equations (15) and (19) respectively.

Method	time	objective	Lagrangian	coincide with steady case
Theory	infinite	Appendix C [22]	By definition	Example 3, Theorems 4, 5
Theory	finite	Appendix C [22]	Theorem 1	Example 3, Theorems 4, 5, 1
Algorithm Ide [22]	infinite	Example 1	Example 2, Theorem 2	Example 3, Theorems 6, 7
Algorithm Ide [22]	finite	Example 1	Example 2, Theorems 2, 1	Example 3, Theorems 6, 7, 1
Algorithm Ju [23]	infinite	Example 1	Theorem 3	Example 3, Theorems 6, 7
Algorithm Ju [23]	finite	Example 1	Theorems 3, 1	Example 3, Theorems 6, 7, 1
Alg. Hofmann [21]	infinite	Section 4.1.3	Theorem 3	Section 4.3.4
Alg. Hofmann [21]	finite	Section 4.1.3	Theorems 3, 1	Section 4.3.4, Theorem 1

Table 1: Summary of the mathematical properties and references to theorems and counter examples for the different settings and algorithms of DHTs. Color represents: green: yes, teal: mostly yes, purple: mostly no, red: no.

Now, we show the non-objectivity by transforming the field through the Galilean transformation $z' = z + \frac{1}{4}t$, which results in

$$u'(z', t) = (z' - \frac{1}{4}t)^2 + z' - \frac{1}{4}t + \frac{1}{4}. \quad (26)$$

The only zero $z'_c(t) = \frac{1}{4}t - \frac{1}{2}$ of this field is not hyperbolic

$$\nabla u'(z'_c, t) = 2z' - \frac{1}{2}t + 1|_{z=z_c} = 0, \quad (27)$$

which causes both algorithms to stop and to not return a result.

As a trivial result, the algorithms by Ide et al. and by Ju et al. are not objective for finite times either.

4.1.3 Algorithm by Hofmann et al.

The algorithm by Hofman et al. [21] cannot be fooled as in Example 1 if it uses steadified initial guesses. With the version by Machado et al. [28], it becomes Galilean invariant but not objective. With the version by Rojo et al. [35], it becomes objective.

There are two restrictions though. First the algorithm by Rojo et al. does not work if the localized field is linear. Second, the filtering of the initial guesses w.r.t. very small Jacobian determinant $|\nabla u(z_c, t)| \ll 0$ makes the algorithm not objective but only Galilean invariant, like the Jacobian.

4.2 Lagrangianness

We call a method Lagrangian if the features it extracts move over time as if they were advected by the flow $v(x, t)$. For line features $x(t) : \mathbb{R} \rightarrow \mathbb{R}^2$, this is equivalent to the extracted line to be a pathline, i.e., a trajectory, i.e., tangential to the flow $\forall t \in \mathbb{R} : \dot{x}(t) = v(x(t), t)$.

4.2.1 Theory

DHTs are trajectories by definition, i.e., they are Lagrangian.

4.2.2 Finite Time

Ide et al. stress that the extension of the data to infinite times from Section 3.2.5 does generally not return the correct DHT, but under the following condition, the result is tangential to the given data.

Theorem 1. *If $g : [t_0, t_1] \subset \mathbb{R} \rightarrow \mathbb{R}^2$ is extended to infinity through $\tilde{g}(t) : \mathbb{R} \rightarrow \mathbb{R}^2$ such that it coincides with its extension perfectly for the time interval the data is given, i.e., $\forall t \in [t_0, t_1] : \tilde{g}(t) = g(t)$, then the approximate DHT is a trajectory.*

4.2.3 Algorithm by Ide et al.

The algorithm by Ide et al. is not always Lagrangian.

Example 2. *This example shows a case in which the algorithm by Ide et al. does not return a pathline. Neglecting the non-linear term in the case of the 1D vector field*

$$\dot{x} = v(x, t) = x + t + x^2, \quad (28)$$

which is the last part in the first step of the algorithm described in Section 3.2.2, leads to

$$\dot{y} = u(y, t) = y + t. \quad (29)$$

Its solutions are the trajectories of equation (29), $y(y_0, t) = e^t(y_0 + 1) - t - 1$, of which $y^{DHT} = y(-1, t) = -t - 1$ is the DHT. But its tangent $\dot{y}^{DHT} = -1$ does not point along the original vector field (28) because $v(x^{DHT}(t), t) = x^{DHT} + t + x^{DHT^2} = -1 + (-t - 1)^2$. Therefore the line that is detected is not a pathline. See Appendix Fig 5 for illustration.

The algorithm does not always provide a solution even if it exists in theory, e.g., Example 1. But if it has a finite result for the input vector field of the shape (14), that result is Lagrangian.

Theorem 2. *If the algorithm returns a solution for a linear system in space (14), then this solution is a pathline.*

A proof using the analytical solution can be found in the Appendix. It follows from combining the results in this section that the algorithm by Ide et al. is Lagrangian for finite time if the series approximation to $g(t)$ is perfect for all $t \in [t_0, t_1]$ and the input field is linear in space.

4.2.4 Algorithm by Ju et al. and Hofmann et al.

All three algorithms do not always converge to a solution even if it exists in theory, because the integration of the fundamental matrix and its SVD are prone to numerical error [21–23] even in the decomposed forms. But if the latter two converge to a fixpoint, the result is a pathline.

Theorem 3. *Every trajectory of $\dot{y} = Dy + g(y, t)$ is a fixpoint of equation (19) and vice versa.*

A proof using the Leibnitz rule can be found in the Appendix. Since Ju et al. and Hofmann et al. use a zero extension outside the given time interval, their method satisfies the conditions of Theorem 1 and is therefore always Lagrangian if it converges.

4.3 Coincidence with the Steady Vector Field Topology

In this subsection, we will answer the question whether or not DHTs coincide with critical points on steady velocity fields. Mathematically speaking, suppose we have an unsteady flow field $\bar{u} : \mathbb{R}^2 \times \mathbb{R} \rightarrow \mathbb{R}^2$ that is defined over space and time, but does not change over time, i.e., there exists a steady field $u : \mathbb{R}^2 \rightarrow \mathbb{R}^2$ such that $\forall t \in \mathbb{R} : \bar{u}(z, t) = u(z)$. Then we want the DHTs $z^{DHT}(t)$ extracted in \bar{u} to satisfy $\bar{u}(z^{DHT}(t)) = u(z^{DHT}(t)) = 0$.

4.3.1 Theory

Not every classical critical point is a DHT even in theory.

Example 3. *The classical steady center is not a DHT. The critical point $y_c = (0, 0)^T$ in the steady vector field*

$$\dot{y} = \begin{pmatrix} y_2 \\ -y_1 \end{pmatrix} \quad (30)$$

shown in Figure 1(e) has a Jacobian whose eigenvalues $\lambda_{1/2} = \pm i$ have zero real part, which makes y_c not hyperbolic and therefore not a DHT.

But DHTs of steady fields are critical points and some critical points are DHTs, especially, all critical points in Figure 1 except for the center.

Theorem 4. *A critical point with a non-defective full rank Jacobian is a DHT.*

Theorem 5. *A DHT in a steady field is an isolated critical point.*

4.3.2 Finite Time

If a constant field is given as a finite-time dataset that happens to not change over time, then the expansion using a power series or a Fourier series can always be made perfect on the given finite-time interval just by using the zeroth-order approximation. That means the finite time DHTs coincide with the infinite time DHTs because of Theorem 1.

4.3.3 Algorithms by Ide et al. and Ju et al.

Both algorithms detect hyperbolic critical points in steady fields.

Theorem 6. *A critical point with a non-defective full rank Jacobian is detected as a DHT through the algorithms by Ide et al. [22] and Ju et al. [23].*

Theorem 7. *A DHT detected through the algorithm by Ide et al. [22] or Ju et al. [23] in a steady field is a critical point.*

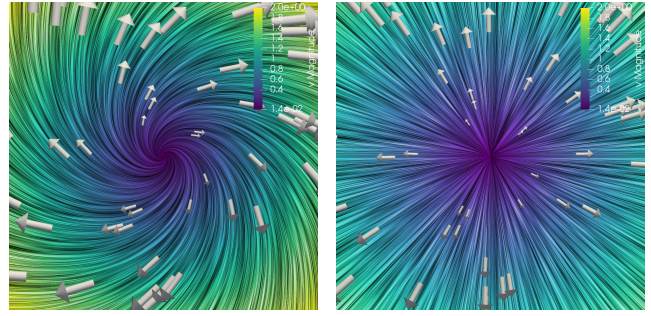
4.3.4 Algorithm by Hofmann et al.

Both considered steadification algorithms leave a steady input field unchanged [7]. Therefore the algorithm inherits its properties mostly from the one by Ju et al., except for the fact that Hofmann et al. suggest filtering out initial guesses with positive Jacobian determinant, removing sinks and sources. Omitting the filtering step makes this algorithm detect the same critical points as the one by Ju et al..

5 VISUALIZATION OF DISTINGUISHED TRAJECTORIES

We have seen that DHTs generalize critical points to the time-dependent setting in a physically meaningful way in some cases, but not in all.

If we require a method to be Lagrangian, the generalized critical points must be pathlines. Because of that, we treat the visualization of distinguished trajectories and not necessarily DHTs to generalize critical points in this section. By distinguished trajectories, we mean isolated pathlines of the data that generalize critical points. That means our method can visualize multiple trajectories simultaneously, but we expect them to be separated. They can be DHTs, but they do not have to be. With this approach, we allow our visualization to also cover future developments in the theory of time-dependent flow topology that might, for example, be able to also detect centers.



(a) Input vector field (31).

(b) Decoupled vector field (33).

Figure 2: An example where a steady input field does not remain unchanged through the transformation in Section 3.2.3.

5.1 Problem Statement

Given a time-dependent input velocity field $v(x, t)$ and a distinguished trajectory $x(t)$, we want to find a coordinate transformation $y = A(t)x + b(t)$ that allows us to perceive the field from the perspective of the trajectory. We especially want the trajectory to become a critical point for all times. An example can be found in Fig. 3.

We will first show that this requirement is not met by the transformation from Section 3.2.3 and then derive a similar transformation that satisfies it. We will also show that the result satisfies Lagrangian-ness and objectivity.

5.2 Making the Trajectory the Critical Point

The first goal of making the trajectory critical can be achieved very easily through the transformation (5) that is used for the detection of the DHTs to localize around a line $x' = x - x(t)$. Note that localization of a steady field around a non-steady line $x(t)$ can result in an unsteady field, but all Euclidean markers in a steady field are steady.

5.3 Steadification and Diagonalization of the Jacobian

A straightforward idea to define the “natural” reference frame of a trajectory is through transformation (9), which decouples the dynamical system. It is promising because it also allows us to express the data independently of time, but it comes with two drawbacks. First, as we have seen, this transformation only exists for hyperbolic trajectories, which are not powerful enough to generalize all critical points. Second, even if it exists, it does not generally coincide with the input field, even if that is steady.

Example 4. *The transformation $y = A(t)x$ as derived in Section 3.2.3 for the steady field*

$$\dot{x} = \begin{pmatrix} x_1 + x_2 \\ x_2 - x_1 \end{pmatrix} \quad (31)$$

shown in Figure 2 with $t_0 = 0$ is actually not constant over time

$$A(t) = \begin{pmatrix} \cos(t) & \sin(t) \\ -\sin(t) & \cos(t) \end{pmatrix}, \quad (32)$$

but it produces the steady decoupled form

$$\dot{y} = \begin{pmatrix} y_1 \\ y_2 \end{pmatrix}, \quad (33)$$

which does not coincide with the input system (31).

We will now derive a transformation that overcomes both drawbacks.

5.4 Steadification of the Antisymmetric Jacobian

In this section, we derive a transformation that is similar to the one in Section 3.2.3, but differs from it in two ways. First, it exists for any non-degenerate localization of the form (8) and not only for hyperbolic trajectories. Second, it leaves steady fields unchanged. It further satisfies the second visualization goal and returns a steady field if the unsteady field happens to be a moved steady field.

The symmetric part of the Jacobian is objective, while the antisymmetric part is not. We chose a transformation that makes the antisymmetric part steady.

Theorem 8. *Let $\dot{x} = v(x, t) : \mathbb{R}^2 \times \mathbb{R} \rightarrow \mathbb{R}^2$ be a flow field that has been localized around a trajectory as in Section 5.2, i.e., it has a critical point in the center of coordinates $v(0, t) = 0$. Then the time-dependent rotation*

$$Q(r(t)) = \begin{pmatrix} \cos(r(t)) & -\sin(r(t)) \\ \sin(r(t)) & \cos(r(t)) \end{pmatrix} \quad (34)$$

with the function $r(t) : \mathbb{R} \rightarrow \mathbb{R}$ satisfying the initial value problem

$$\ddot{r}(t) = \frac{1}{2}(\dot{j}_{0,1}(t) - \dot{j}_{1,0}(t)), \quad r(t_0) = 0, \quad \dot{r}(t_0) = 0, \quad (35)$$

where $j_{k,l}(t)$ are the matrix entries of the Jacobian $J = \nabla v$, provides a transform $y = Q(t)x$ such that the output field $\dot{y} = Q\dot{x} + \dot{Q}x$ is objective and coincides with the input field $v(x, t)$ if that is steady.²

Proof. We first show the coincidence with the steady case. If the input field $\dot{x} = v(x)$ is steady, then the Jacobian is, too; its derivative vanishes, and equation (35) simplifies to $\ddot{r}(t) = 0$ with the analytical solution $r(t) = c_1 t + c_0$. The initial values require $c_0 = r(t_0) = 0$ and $c_1 = \dot{r}(t_0) = 0$, which leads to $r(t) = 0$, $Q(r(t)) = I$, and $\dot{y} = \dot{x} = v(x) = v(y)$.

Now we show the objectivity. We only have to look at transformations of the form $x' = Q(t)x$ because the translational part has already been taken care of in Section 5.2.

We will make use of the fact that for the rotation matrix (34), the following matrix products are antisymmetric and satisfy

$$Q^T \dot{Q} = \begin{pmatrix} 0 & -\dot{r} \\ \dot{r} & 0 \end{pmatrix}, \quad Q^T \ddot{Q} + \dot{Q}^T \dot{Q} Q^T = \begin{pmatrix} 0 & -\ddot{r} \\ \ddot{r} & 0 \end{pmatrix}. \quad (36)$$

Assume we have two velocity fields $\dot{x} = v(x, t)$ and

$$v'(x', t) = \dot{x}' = \dot{Q}(t)x + Q(t)\dot{x} = \dot{Q}(t)x + Q(t)v(x', t) \quad (37)$$

that differ by a transform $x' = Q(t)x$ with the rotation matrix $Q(s(t))$ as in equation (34) with some function $s : \mathbb{R} \rightarrow \mathbb{R}$. Then their Jacobians satisfy $J = \nabla v$ and

$$\begin{aligned} J'(x', t) &= \nabla_{x'} v'(x', t) \\ &= \dot{Q}(t) \nabla_x x Q^T(t) + Q(t) \nabla_x v(x', t) Q^T(t) \\ &= \dot{Q}(t) Q^T(t) + Q(t) J(x', t) Q^T(t) \end{aligned} \quad (38)$$

and the temporal derivative of the Jacobians

$$\begin{aligned} J' &= \dot{Q} Q^T + \dot{Q} \dot{Q}^T + \dot{Q} J Q^T + Q J \dot{Q}^T + Q J \dot{Q}^T \\ &= Q(Q^T \dot{Q} + \dot{Q}^T \dot{Q} Q^T + Q^T \dot{Q} J + J + J \dot{Q}^T Q) Q^T \\ &\stackrel{(36)}{=} Q \left(\begin{pmatrix} 0 & -\dot{s} \\ \dot{s} & 0 \end{pmatrix} + J \right) Q^T. \end{aligned} \quad (39)$$

It is apparent that s leaves the symmetric part $\frac{1}{2}(J + J^T)$ of J unchanged, which is in accordance with the fact that this tensor is

²By objective we mean that two input vector fields that differ only by a change of reference frame produce the same output field.

objective, but only influences the antisymmetric part $\frac{1}{2}(J - J^T)$ of J . And the one-dimensional second order ordinary differential equation (35) is chosen exactly to let the antisymmetric part inside the parentheses vanish.

The antisymmetric parts satisfy

$$\frac{1}{2}(J' - J'^T) \stackrel{(35)}{=} Q \left(\begin{pmatrix} 0 & -\ddot{s} \\ \ddot{s} & 0 \end{pmatrix} + \begin{pmatrix} 0 & -\ddot{r} \\ \ddot{r} & 0 \end{pmatrix} \right) Q^T. \quad (40)$$

Therefore we get the initial value problem

$$\dot{r}'(t) = \ddot{s} + \ddot{r}, \quad r'(0) = s(0), \quad \dot{r}'(0) = \dot{s}(0) \quad (41)$$

with the solution $r'(t) = s(t) + r(t)$ that leads to $Q(r') = Q(r)Q(s)$ through straight calculation and completes the proof through $y' = Q(r')x' = Q(r)Q(s)x' = Q(r)x = y$. \square

Note that the transformation is well defined for any input vector field. In particular it does not need to have a linear part. A proof for reflections works analogously.

5.5 Generalization to Arbitrary Paths

Note that we did not use the fact that $x(t)$ is a trajectory for the visualization, but only to ensure that the method is Lagrangian. The method can be used to visualize a flow field from the perspective of arbitrary paths, too, for example, to show the iterations in the algorithm by Ju et al. [23].

5.6 Visualization

We follow two main goals for the visualization. We seek to

- show the movement of the trajectory over time, and
- emphasize the analogy to the steady vector field topology

because vector field topology has been broadly accepted as an excellent way to visualize steady fields to the degree that the phase portraits around critical points have an almost iconic recognition value in scientific visualization.

5.6.1 Trajectory

For the first goal, we chose to draw the path of the distinguished trajectory over the whole time interval in the original frame of reference. We interpolate a trajectory that is given at the discrete time steps using a spline to make it visually appealing.

For the temporal coherence of the visualization, we color code it blue for times that lie in the past w.r.t. the currently displayed time step and red for times that lie in the future. The saturation of the colors increases with the difference in time. Our algorithm uses the Visualization Toolkit VTK [37] and stores the trajectory as time-dependent vtkPolyData with a scalar array that contains the time distance of the point on the trajectory to the current time step. That way, it can easily be visualized with a transfer function in a standard visualization environment, such as ParaView [1].

A second cue for the speed in which the trajectory moves is provided through ticks on the curve of the trajectory at every timestep. We achieve that by storing cells of the type vtk.Vertex only at the discrete time steps and not on the interpolated points between them. This provides the temporal context of the evolution of the trajectory; see Figure 3.

We seek to ensure that the context does not occlude the visualization of the instantaneous velocity field in the perspective of the trajectory from the second goal. Therefore we render the trajectory transparent in the vicinity of its location in the current time step. We set the time distance array to zero for all points that are closer to the current location of the trajectory than one cell size so that a recirculating trajectory will not occlude the visualization. An example of this effect can be seen in Figure 3(f), where the trajectories of the first and last time step coincide.

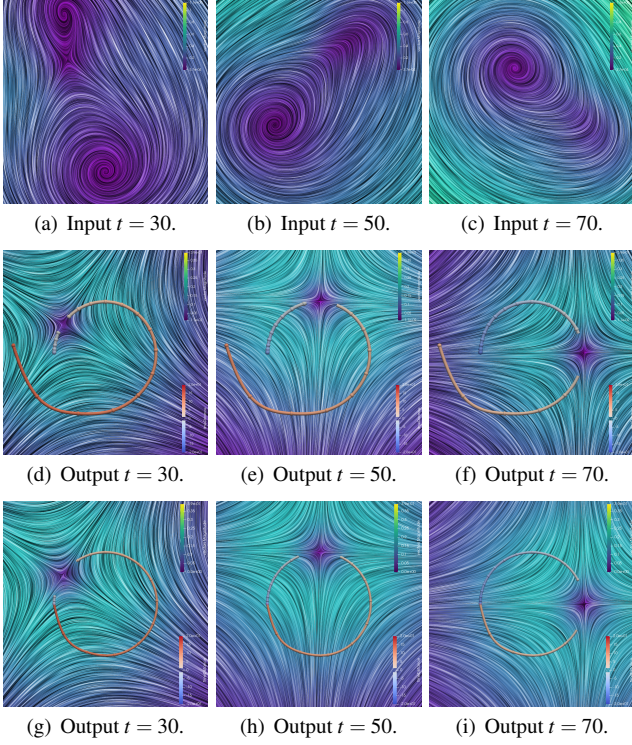


Figure 3: Top row: different time steps of the saddle (44) under the accelerated rotation visualized using LIC. Middle row: the trajectory of the approximate DHT computed with the algorithm by Ju et al. over time on top of the instantaneous velocity of the field from its perspective as derived through our algorithm in Section 5.7. Bottom row: the trajectory of the true DHT (45) on top of the instantaneous velocity of the field from the DHT’s perspective.

5.6.2 Instantaneous Velocity

Let a field $v(x, t)$ be just a steady field v_s moved through a Euclidean transformation $x' = A(t)x + b(t)$, i.e., a field with the shape

$$v(x, t) = \dot{A}(t)A^T(t)(x - b(t)) + A(t)v_s(A^T(t)(x - b(t))) + \dot{b}(t), \quad (42)$$

and $x'_c(t)$ a trajectory $x'_c(t) = Q(t)x_c + r(t)$ that describes the movement of a critical point $v_s(x_c) = 0$. The requirement that for this input, $v(x, t), x'_c(t)$, we want the original field v_s back is not a well-defined problem, because all constant Euclidean transformations of a steady field are also steady. Analogously to the field decomposition suggested by Rojo et al. [35], we attribute special meaning to the lab frame and visualize the derived field

$$w(x, t) := v(x, t) - \dot{Q}^T(r(t))Q(r(t))(x - x'_c(t)) - v(x'_c(t)), \quad (43)$$

whose critical points follow the trajectory in the lab frame $w(x'_c(t), t) = 0$. The choice $r(t_0) = 0$ determines the rotational alignment selecting the representative v_s that satisfies $A(t_0) = I$. In the case of the transformed field (42), we get $A(t)A(t_0)^{-1} = Q(r(t))^T$ from Section 5.4. Together with $b(t) = -x'_c(t)$, we see that the derived field (43) really shows the rotated and shifted steady field $Q(r(t))v_s(Q^T(r(t))(x' - r(t)), t)$ without the “fictitious forces” $\dot{Q}(t)Q^T(t)(x - r(t))$ and $\dot{r}(t)$ that come from the derivatives of the transformation.

After computing the transformation in Section 5.4, we compute $w(x, t)$ from equation (43) and visualize it using line integral convolution (LIC) [8] color coded by the velocity magnitude in each time step. Please note that in general all visualization methods that are suitable for steady vector fields can be used instead of the LIC.

5.7 Algorithm

The steps in this section can be summarized by the following algorithm.

1. Select the distinguished trajectory $x(t) = F_{t_0}^t(x_0)$.
2. Make the trajectory critical through the transform $x' = x - x(t)$.
3. If the field is steady, return $r(t) = 0$, otherwise solve $\dot{r}(t) = \frac{1}{2}(J_{0,1} - J_{1,0})$ using a Runge-Kutta method.
4. Steadify the antisymmetric part of the localization around the trajectory through the transform $x'' = Q(r(t))x'$ with Q from equation (34).
5. Compute the velocity field $w(x, t) = v(x, t) - v(x(t), t) - \dot{Q}^T Q(x - x(t))$ showing v from the perspective of x .

5.8 Multiple Distinguished Trajectories

If a flow field has multiple distinguished trajectories, each provides one view of the field. Distinguished hyperbolic trajectories are separated. We can therefore visualize a number of their paths simultaneously and let the observer switch between them for the localized steadified flow. Their separatedness also allows us to visualize several localized flows in one image similar to Fuchs et al. [11] and Bujack et al. [6] using inverse distance weighting [38]. The exponent p in the interpolation scheme allows the user to steer the smoothness. For $p = \infty$, we get the largest possible cutout of the undisturbed reference frame of each trajectory with a non-smooth transition between the patches. For smaller p , the results become smoother, but in return, the mix of the frames of reference lets the velocity lose meaning away from the trajectories.

6 RESULTS

In this section, we showcase the combination of the algorithms by Ju et al. [23] and ours from Section 5.7 for two simple analytical examples for which the former converges.

6.1 Saddle under Accelerated Rotation

To demonstrate the coincidence with the steady case and the objectivity, we use an analytical, steady dataset that is moved through a Euclidean transformation, for which we know ground truth. We chose a saddle

$$v_s(x) = \begin{pmatrix} x_1 + 0.5 \\ -x_2 \end{pmatrix} e^{-2\sqrt{(x_1 + 0.5)^2 + x_2^2}} \quad (44)$$

that is rotated with increasing velocity clockwise once around the circle with radius 0.5 and center $(0, 0, 0)^T$ through the matrix (34) with the function $r(t) = \theta t^2$ with $\theta = \frac{2\pi}{|N|^2}$ chosen to make one full turn in $N = 20$ time steps. The critical point $x_c = (-0.5, 0)^T$ is transformed to

$$x'_c(t) = A(t)x_0 = \frac{1}{2} \begin{pmatrix} -\cos(\theta t^2) \\ \sin(\theta t^2) \end{pmatrix}, \quad (45)$$

which is the true location of the DHT.

The transformed field has one hyperbolic critical point that remains in the spatial boundaries that vanishes at time step 35. We use a path as input that follows the critical point in the beginning and then continues as its pathline as the input to the algorithm by Ju et al. The algorithm converges and provides an approximate DHT, which does not fully coincide with the location of the true DHT (45). Still, visualizing the flow in the frame of reference of the approximate DHT using our algorithm from Section 5.7 reveals the true type and orientation of the rotating saddle through the instantaneous velocity field in each time step. Simultaneously, the visualization of the trajectory provides the path of the DHT for over all time steps with the increasing distance between the ticks and color coding revealing

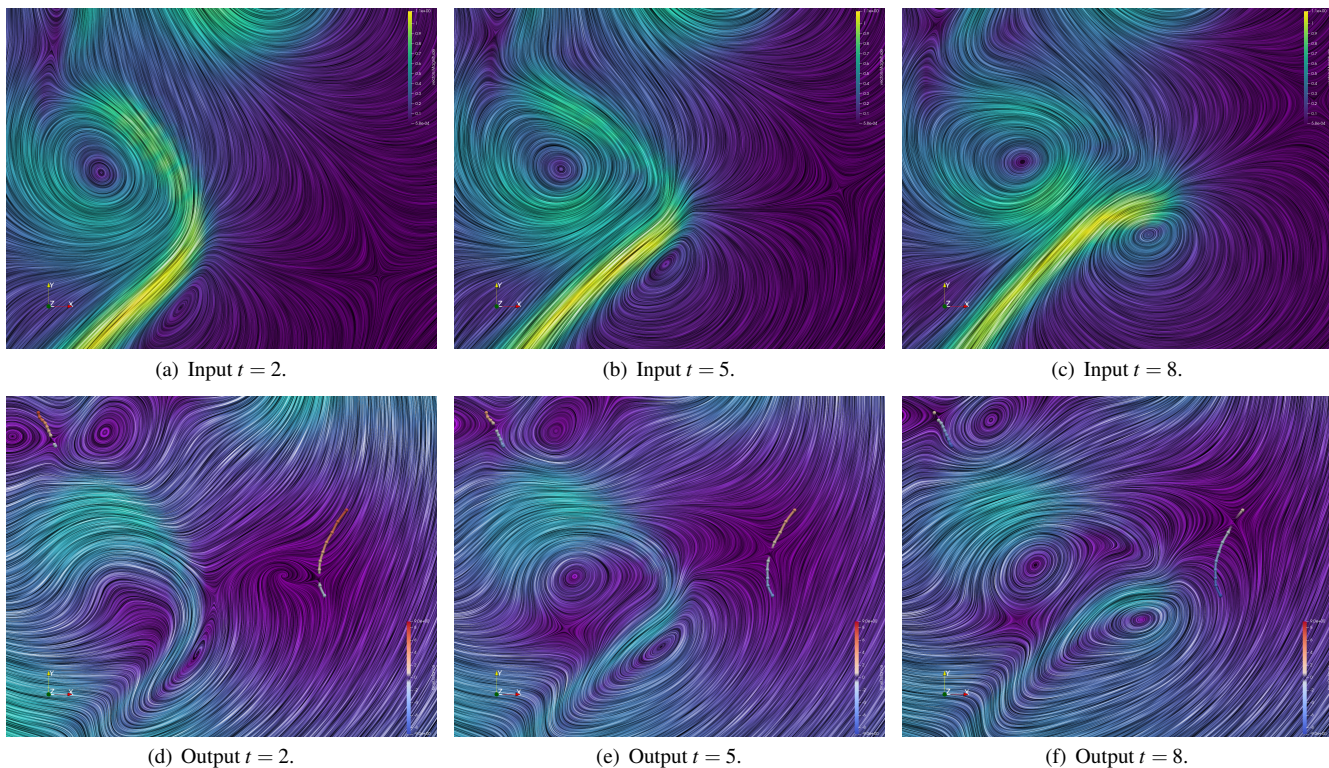


Figure 4: Top row: different time steps of the jet entering a fluid at rest visualized using LIC. Bottom row: the trajectory of the DHTs over time on top of the instantaneous velocity of the field from the DHTs’ perspectives as derived through our algorithm in Section 5.7.

its exact location in each time step. Together, this intuitively reveals the underlying nature of that the dataset, namely that it is a steady saddle that is rotated in a circle with increasing speed. The reader is encouraged to refer to the supplementary video for an animation.

6.2 Jet Entering Fluid at Rest

We demonstrate that our visualization can be applied to several input trajectories for the example of hydrodynamics simulation data of a swirling jet entering a fluid at rest. The top row of Fig 4 shows two saddles that persist over a longer period of time, one in the top left and one in the bottom right moving upward. We use their paths as initial guesses for the algorithm suggested by Ju. It converges to the two trajectories in the bottom of Fig. 4. The vector field in the background uses inverse distance weighting with an exponent of $p = 2$ between the two reference frames that correspond to each of the distinguished hyperbolic trajectories. The visualization not only reveals the path of the DHTs, but also the velocity profile around it in exactly the same way we interpret it around critical points in the classical vector field topology. Only now do we know that the results are physically meaningful because they are in accordance with the pathlines in the time-dependent flow.

7 DISCUSSION AND CONCLUSION

So far, there is no visualization algorithm that generalizes classical vector field topology to the time-dependent setting that satisfies the three desirable properties: Lagrangianness, objectivity, and coincidence with the classical case, which are frequently considered necessary to ensure physical meaning.

We have analyzed DHTs with respect to these three conditions and shown that DHTs are theoretically Lagrangian and objective, but do not coincide with the steady case in all cases, especially if the Jacobian around the trajectory is not diagonalizable. Analyzing the algorithms for their detection has shown that they have improved

over time. The first one by Ide et al. is not generally objective or Lagrangian. The developments by Ju et al. ensure Lagrangianness and the algorithm by Hofmann et al. can be made objective with small adaptations. This makes it theoretically superior to all previous algorithms [7], none of which achieved all three properties. The strongest contenders were the steadification algorithms, which lack Lagrangianness, and the pathline categorization algorithms, which lack being a true generalization of critical points. The main challenges remaining to overcome are the algorithms’ numerical sensitivity and cases where they do not converge.

Further, we have provided a visualization for DHTs that is to the best of our knowledge the first to theoretically generalize non-degenerate critical points with non-defective Jacobian of analytic flow fields to the time-dependent setting in a physically meaningful way, i.e., it is Lagrangian and objective. The visualization itself works for any distinguished trajectory and is therefore ready to satisfy all three desirable properties as soon as the algorithms advance to enable the detection of non-diagonalizable critical points in a Lagrangian way.

We hope that identifying the differences between the expected results and the actual capabilities of the existing algorithms will help closing those gaps in the future. Also, we hope that it inspires analogous analysis for separatrices, periodic orbits, and 3D flows.

ACKNOWLEDGMENTS

We gratefully acknowledge the support of the U.S. Department of Energy through the Los Alamos National Laboratory’s Laboratory Directed Research and Development Program under project number 20190143ER for this work. This work is published under LA-UR-20-23159.

REFERENCES

- [1] J. Ahrens, B. Geveci, and C. Law. Paraview: An end-user tool for large-data visualization. *The Visualization Handbook*, pp. 717–731, 2005.
- [2] M. Branicki and S. Wiggins. An adaptive method for computing invariant manifolds in non-autonomous, three-dimensional dynamical systems. *Physica D: Nonlinear Phenomena*, 238(16):1625–1657, 2009.
- [3] M. Branicki and S. Wiggins. Finite-time Lagrangian transport analysis: stable and unstable manifolds of hyperbolic trajectories and finite-time Lyapunov exponents. *Nonlinear Processes in Geophysics*, 17(1):1–36, 2010.
- [4] R. Bujack, S. Dutta, I. Baeza Rojo, D. Zhang, and T. Günther. Objective Finite-Time Saddles and their Connection to FTLE. In J. Johansson, F. Sadlo, and G. E. Marai, eds., *EuroVis 2019 - Short Papers*, pp. 49–53. The Eurographics Association, 2019.
- [5] R. Bujack, S. Dutta, D. Zhang, and T. Günther. Objective finite-time flow topology from flowmap expansion and contraction. In *Topological Methods in Data Analysis and Visualization VI*, pp. 111–131. Springer, 2021.
- [6] R. Bujack, M. Hlawitschka, and K. I. Joy. Topology-Inspired Galilean Invariant Vector Field Analysis. In *Proceedings of the IEEE Pacific Visualization Symposium, PacificVis 2016 in Taipei, Taiwan*, pp. 72–79, 2016.
- [7] R. Bujack, L. Yan, I. Hotz, C. Garth, and B. Wang. State of the art in time-dependent flow topology: Interpreting physical meaningfulness through mathematical properties. In *Computer Graphics Forum*, vol. 39, pp. 811–835. Wiley Online Library, 2020.
- [8] B. Cabral and L. C. Leedom. Imaging vector fields using line integral convolution. In *Proceedings of the 20th annual conference on Computer graphics and interactive techniques, SIGGRAPH '93*, pp. 263–270. ACM, 1993. doi: 10.1145/166117.166151
- [9] C. Chicone. *Ordinary differential equations with applications*, vol. 34. Springer Science & Business Media, 2006.
- [10] W. A. Coppel. *Dichotomies in stability theory*, vol. 629. Springer, 2006.
- [11] R. Fuchs, J. Kemmler, B. Schindler, J. Waser, F. Sadlo, H. Hauser, and R. Peikert. Toward a Lagrangian vector field topology. In *Computer Graphics Forum*, vol. 29, pp. 1163–1172. Wiley Online Library, 2010.
- [12] C. Garth, X. Tricoche, and G. Scheuermann. Tracking of vector field singularities in unstructured 3d time-dependent datasets. In *Visualization, 2004. IEEE*, pp. 329–336. IEEE, 2004.
- [13] T. Germer, M. Otto, R. Peikert, and H. Theisel. Lagrangian coherent structures with guaranteed material separation. 30(3):761–770, 2011.
- [14] T. Günther, M. Gross, and H. Theisel. Generic objective vortices for flow visualization. *ACM Transactions on Graphics (TOG)*, 36(4):141, 2017.
- [15] M. Hadwiger, M. Mlejnek, T. Theußl, and P. Rautek. Time-dependent flow seen through approximate observer killing fields. *IEEE transactions on visualization and computer graphics*, 25(1):1257–1266, 2018.
- [16] G. Haller. Finding finite-time invariant manifolds in two-dimensional velocity fields. *Chaos: An Interdisciplinary Journal of Nonlinear Science*, 10(1):99–108, 2000.
- [17] G. Haller. Lagrangian Coherent Structures from Approximate Velocity Data. *Physics of Fluids*, 14:1851–1861, 2002.
- [18] C. Heine, H. Leitte, M. Hlawitschka, F. Iuricich, L. De Florian, G. Scheuermann, H. Hagen, and C. Garth. A survey of topology-based methods in visualization. *Computer Graphics Forum*, 35(3):643–667, 2016.
- [19] J. Helman and L. Hesselink. Representation and display of vector field topology in fluid flow data sets. *Computer*, 22(8):27–36, 1989.
- [20] J. L. Helman and L. Hesselink. Surface representations of two-and three-dimensional fluid flow topology. In *Proceedings of the 1st conference on Visualization '90*, pp. 6–13. IEEE Computer Society Press, 1990.
- [21] L. Hofmann and F. Sadlo. Extraction of distinguished hyperbolic trajectories for 2d time-dependent vector field topology. 39(3):303–315, 2020.
- [22] K. Ide, D. Small, and S. Wiggins. Distinguished hyperbolic trajectories in time-dependent fluid flows: analytical and computational approach for velocity fields defined as data sets. *Nonlinear Processes in Geophysics*, 9(3/4):237–263, 2002.
- [23] N. Ju, D. Small, and S. Wiggins. Existence and computation of hyperbolic trajectories of aperiodically time dependent vector fields and their approximations. *International Journal of Bifurcation and Chaos*, 13(06):1449–1457, 2003.
- [24] J. Kasten, I. Hotz, B. R. Noack, and H.-C. Hege. On the extraction of long-living features in unsteady fluid flows. In V. Pascucci, X. Tricoche, H. Hagen, and J. Tierny, eds., *Topological Methods in Data Analysis and Visualization*, Mathematics and Visualization, pp. 115–126. Springer Berlin Heidelberg, 2011. doi: 10.1007/978-3-642-15014-2_10
- [25] J. Kasten, J. Reininghaus, I. Hotz, H.-C. Hege, B. R. Noack, G. Daviller, and M. Morzynski. Acceleration feature points of unsteady shear flows. *Archives of Mechanics*, 68:55–80, 2016.
- [26] R. S. Laramée, G. Chen, M. Jankun-Kelly, E. Zhang, and D. Thompson. Bringing topology-based flow visualization to the application domain. *Topology-Based Methods in Visualization II Mathematics and Visualization*, 2009.
- [27] R. S. Laramée, H. Hauser, L. Zhao, and F. H. Post. Topology-based flow visualization, the state of the art. In H. Hauser, H. Hagen, and H. Theisel, eds., *Topology-based Methods in Visualization*, pp. 1–19, 2007.
- [28] G. Machado, S. Boblest, T. Ertl, and F. Sadlo. Space-time bifurcation lines for extraction of 2d Lagrangian coherent structures. In *Computer Graphics Forum*, vol. 35, pp. 91–100. Wiley Online Library, 2016.
- [29] A. Mancho, D. Small, and S. Wiggins. Computation of hyperbolic trajectories and their stable and unstable manifolds for oceanographic flows represented as data sets. 2004.
- [30] A. M. Mancho, S. Wiggins, J. Curbelo, and C. Mendoza. Lagrangian descriptors: A method for revealing phase space structures of general time dependent dynamical systems. *Communications in Nonlinear Science and Numerical Simulation*, 18(12):3530–3557, 2013.
- [31] J. J. Palis and W. De Melo. *Geometric theory of dynamical systems: an introduction*. Springer Science & Business Media, 2012.
- [32] L. Perko. *Differential equations and dynamical systems*, vol. 7. Springer Science & Business Media, 2013.
- [33] A. Pobitzer, R. Peikert, R. Fuchs, B. Schindler, A. Kuhn, H. Theisel, K. Matkovic, and H. Hauser. The state of the art in topology-based visualization of unsteady flow. *Computer Graphics Forum*, 30(6):1789–1811, 2011.
- [34] J. Reininghaus, J. Kasten, T. Weinkauff, and I. Hotz. Efficient computation of combinatorial feature flow fields. *IEEE Transactions on Visualization and Computer Graphics*, 18(9):1563–1573, 2012.
- [35] I. B. Rojo and T. Günther. Vector field topology of time-dependent flows in a steady reference frame. *IEEE Transactions on Visualization and Computer Graphics*, 26(1), 2020. doi: 10.1109/TVCG.2019.2934375
- [36] F. Sadlo and D. Weiskopf. Time-dependent 2-d vector field topology: An approach inspired by Lagrangian coherent structures. In *Computer Graphics Forum*, vol. 29, pp. 88–100. Wiley Online Library, 2010.
- [37] W. J. Schroeder, B. Lorensen, and K. Martin. *The visualization toolkit: an object-oriented approach to 3D graphics*. Kitware, 2004.
- [38] D. Shepard. A two-dimensional interpolation function for irregularly-spaced data. In *Proceedings of the 1968 23rd ACM National Conference*, pp. 517–524, 1968.
- [39] H. Theisel and H.-P. Seidel. Feature flow fields. In *VisSym*, vol. 3, pp. 141–148, 2003.
- [40] H. Theisel, T. Weinkauff, H.-C. Hege, and H.-P. Seidel. Stream line and path line oriented topology for 2d time-dependent vector fields. In *Proceedings of the conference on Visualization '04*, pp. 321–328. IEEE Computer Society, 2004.
- [41] H. Theisel, T. Weinkauff, H.-C. Hege, and H.-P. Seidel. Topological methods for 2D time-dependent vector fields based on stream lines and path lines. *Visualization and Computer Graphics, IEEE Transactions on*, 11(4):383–394, July 2005. doi: 10.1109/TVCG.2005.68
- [42] X. Tricoche, G. Scheuermann, and H. Hagen. Topology-based visualization of time-dependent 2d vector fields. In *VisSym*, pp. 117–126, 2001.
- [43] X. Tricoche, T. Wischgoll, G. Scheuermann, and H. Hagen. Topology

- tracking for the visualization of time-dependent two-dimensional flows. *Computers & Graphics*, 26(2):249–257, 2002.
- [44] M. Uffinger, F. Sadlo, and T. Ertl. A time-dependent vector field topology based on streak surfaces. *IEEE Transactions on Visualization and Computer Graphics*, 19(3):379–392, 2012.
- [45] B. Wang, R. Bujack, P. Rosen, P. Skraba, H. Bhatia, and H. Hagen. Interpreting galilean invariant vector field analysis via extended robustness. In *Topological Methods in Data Analysis and Visualization*, pp. 221–235. Springer, 2017.
- [46] W. Wang, W. Wang, and S. Li. From numerics to combinatorics: a survey of topological methods for vector field visualization. *Journal of Visualization*, 19(4):727–752, 2016.
- [47] T. Weinkauff, H. Theisel, A. Van Gelder, and A. Pang. Stable Feature Flow Fields. *IEEE Transactions on Visualization and Computer Graphics*, 17(6):770–780, June 2011.
- [48] A. Wiebel, R. Chan, C. Wolf, A. Robitzki, A. Stevens, and G. Scheuermann. Topological flow structures in a mathematical model for rotation-mediated cell aggregation. In *Topological Methods in Data Analysis and Visualization*, pp. 193–204. Springer, 2011.
- [49] A. Wiebel, X. Tricoche, D. Schneider, H. Jaenicke, and G. Scheuermann. Generalized streak lines: Analysis and visualization of boundary induced vortices. *IEEE Transactions on Visualization and Computer Graphics*, 13(6):1735–1742, 2007.
- [50] T. Wischgoll, G. Scheuermann, and H. Hagen. Tracking closed streamlines in time dependent planar flows. In *6th International Fall Workshop on Vision, Modeling, and Visualization, VMV 2001*, pp. 447–454, 2001.

APPENDIX

A PROOF OF THEOREM 1

If $g : [t_0, t_1] \subset \mathbb{R} \rightarrow \mathbb{R}^2$ is extended to infinity through $\tilde{g}(t) : \mathbb{R} \rightarrow \mathbb{R}^2$ such that it coincides with its extension perfectly for the time interval the data is given, i.e., $\forall t \in [t_0, t_1] : \tilde{g}(t) = g(t)$, then the approximate DHT is a trajectory.

Proof. Since, y^{DHT} is a DHT of $\dot{y} = Dy + \tilde{g}(t)$, it is a trajectory satisfying

$$\dot{y}^{DHT} = Dy + \tilde{g}(t) = Dy + g(t) \quad (46)$$

for all $t \in [t_0, t_1]$, which makes it Lagrangian. \square

B PROOF OF THEOREM 2

If the algorithm returns a solution for a linear system in space (14), then this solution is a pathline.

Proof. We first show that the DHTs of the system (14) are pathlines. Separation of variables provides the solutions of (14) as

$$y_i(y^0, t) = \int_{t_0}^t g_i(\tau) e^{D_{ii}(t-\tau)} d\tau + y_i^0 e^{D_{ii}(t-t_0)}, \quad (47)$$

which contains the DHTs from (15). We show it for $D_{ii} > 0$ through

$$\begin{aligned} y_i(y^{DHT}(t_0), t) &\stackrel{(47)}{=} \int_{t_0}^t g_i(\tau) e^{D_{ii}(t-\tau)} d\tau + y_i^{DHT}(t_0) e^{D_{ii}(t-t_0)} \\ &= \int_{t_0}^{\infty} g_i(\tau) e^{D_{ii}(t-\tau)} d\tau + y_i^{DHT}(t_0) e^{D_{ii}(t-t_0)} - \int_t^{\infty} g_i(\tau) e^{D_{ii}(t-\tau)} d\tau \\ &\stackrel{(15)}{=} \int_{t_0}^{\infty} g_i(\tau) e^{D_{ii}(t-\tau)} d\tau + \int_{t_0}^{\infty} g_i(\tau) e^{D_{ii}(t_0-\tau)} d\tau e^{D_{ii}(t-t_0)} + y^{DHT}(t) \\ &= y^{DHT}(t). \end{aligned} \quad (48)$$

If a transformation (9) $y = A(t)x$ can be found that makes the system matrix of equation (8) diagonal and constant in time, like in equation (14), then the pathlines of that system are transformed pathlines of the input system because of the frame independence shown in Appendix C in [22], which completes the proof. \square

C PROOF OF THEOREM 3

Every trajectory of

$$\dot{y} = Dy + g(y, t) \quad (49)$$

is a fixpoint of equation (19) and vice versa.

Proof. We show this for the a component with $D_{ii} > 0$ through differentiation of equation (19) for infinite time using the Leibnitz rule at the fixpoint $y^\infty(t)$ via

$$\begin{aligned} \dot{y}_i^\infty(t) &= \frac{d}{dt} \int_{-\infty}^t g_i(y^\infty(\tau), \tau) e^{D_{ii}(t-\tau)} d\tau \\ &= \int_{-\infty}^t \frac{d}{dt} (g_i(y^\infty(\tau), \tau) e^{D_{ii}(t-\tau)}) d\tau + g_i(y^\infty(t), t) e^{D_{ii}(t-t)} \\ &= D_{ii} y_i^\infty(t) + g_i(y^\infty(t), t). \end{aligned} \quad (50)$$

The case with $D_{ii} < 0$ works analogously. \square

D PROOF OF THEOREM 4

A critical point with a non-defective full rank Jacobian is a DHT.

Proof. Localizing the steady field $\dot{z} = v(z)$ around a critical point z_c through $x = z - z_c$ as in Section 3.2.2 results in $\dot{x} = v(x + z_c)$. The second step of the algorithm, Section 3.2.3, linearizes this via

$$\begin{aligned} \dot{x} &= \nabla v(z_c)x + v(x + z_c) - \nabla v(z_c)x \\ &= Fx + h(x). \end{aligned} \quad (51)$$

Since the Jacobian $\nabla v(z_c)$ at the critical point is non-defective, it can be diagonalized through an invertible matrix A and the transform $y = Ax$ leads to

$$\dot{y} = A\dot{x} = AFx + h(x) = AFA^{-1}y + Ah(A^{-1}y) = Dy + g(y), \quad (52)$$

which has the form (4). Since the Jacobian has full rank, none of the diagonal entries vanishes $D_{ii} \neq 0$, which satisfies the condition of hyperbolicity for the constant case.

Since $y_c = Ax_c = 0$ is critical, $y(0, t) = 0$ is a constant trajectory that never leaves any neighborhood around zero. The fact that the trajectories in a neighborhood leave follows from the Hartmann Grobmann theorem [32], which shows that the behavior around a hyperbolic critical point is topologically equivalent to the behavior of its linear part, which in turn satisfies $y^0 e^{Dt}$. This shows that all trajectories leave the neighborhood forward in time along the components where $D_{ii} > 0$ or backward in time where $D_{ii} < 0$, which makes $y^{DHT} = 0$ the DHT. Finally, the back transformation of $y^{DHT} = 0$ leads to $x^{DHT} = A^{-1}y^{DHT} = 0$ and $z^{DHT} = x^{DHT} + z_c = z_c$, which indeed is the critical point of u . \square

E PROOF OF THEOREM 5

A DHT in a steady field is an isolated critical point.

Proof. The Poincare-Bendixon Theorem [32] states that if a trajectory $z(z_0, t)$ is contained in a compact subset $C \subset \mathbb{R}^2$ of the plane, its ω -set either contains a critical point or it is a periodic orbit. If its ω -set is a periodic orbit, then it and its whole interior never leave C , which make neither a DHT. If its ω -set contains a critical point z_c , then $z_c \in C$ is also contained in the compact set and will never leave it because it is critical. Therefore, the only way that $z(z_0, t)$ is the only trajectory remaining in C is if it coincides with z_c . Its isolatedness follows from the fact that all neighboring trajectories must not be constant to leave C . \square

F PROOF OF THEOREM 6

A critical point with a non-defective full rank Jacobian is detected as a DHT through the algorithms by Ide et al. [22] and Ju et al. [23].

Proof. We only have to show that the algorithm returns $y^{DHT} = 0$ for equation (52).

Neglecting the non-linear part in the algorithm by Ide et al. [22] leads to

$$\dot{y} = Dy \quad (53)$$

and equation (15) leads to

$$y_i^{DHT}(t) = \begin{cases} \int_{-\infty}^t 0 e^{D_{ii}(t-\tau)} d\tau, & D_{ii} < 0 \\ -\int_t^{\infty} 0 e^{D_{ii}(t-\tau)} d\tau, & D_{ii} > 0 \end{cases} = 0. \quad (54)$$

The algorithm by Ju et al. [23] also detects $y^{DHT} = 0$, because in the steady case, Equation (19) simplifies to

$$y_i^{j+1} = \begin{cases} g_i(y^j) \int_{-\infty}^t e^{D_{ii}(t-\tau)} d\tau, & D_{ii} > 0 \\ -g_i(y^j) \int_t^{\infty} e^{D_{ii}(t-\tau)} d\tau, & D_{ii} < 0 \end{cases} = -\frac{g_i(y^j)}{D_{ii}}. \quad (55)$$

Starting iteration at the critical point $y^0 = y_c = Ax_c = A(z_c - z_c) = 0$ suffices

$$g(y_c) = g(0) = Ah(0) = A(v(0 + z_c) - \nabla v(x_c)0) = 0, \quad (56)$$

showing that $y_c = 0$ is a fixpoint and the DHT.

Now the back transformation from the proof of Theorem 4 completes the proof in both cases. \square

G PROOF OF THEOREM 7

A DHT detected through the algorithm by Ide et al. [22] or Ju et al. [23] in a steady field is a critical point.

Proof. We first show that no step in the algorithms transforms a steady field into a non-steady field. The localization about the critical point z_c in Section 3.2.3 is constant because the critical point is. Also the transformation to a diagonal matrix in Section 3.2.4 provides constant A, D because we know $\Sigma(t) = Ft$ analytically if F is constant.

Now assume we have detected a DHT in a steady field. After localization about the critical point, equation (14) must suffice $\forall t : g(t) = 0$. Therefore Equations (15) and (19) both return $y^{DHT} = 0$, which coincides with the transformed critical point $y_c = Ax_c = A(z - z_c)$. \square

H ADDITIONAL ILLUSTRATIONS OF EXAMPLES

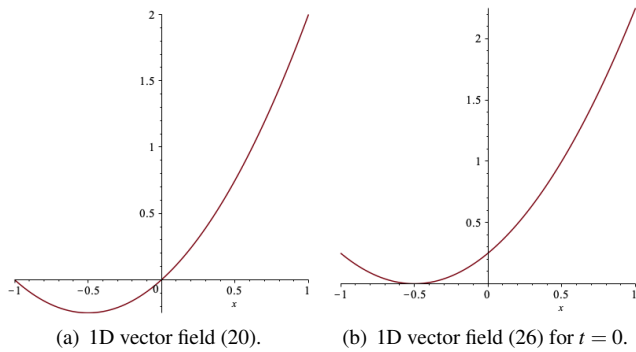
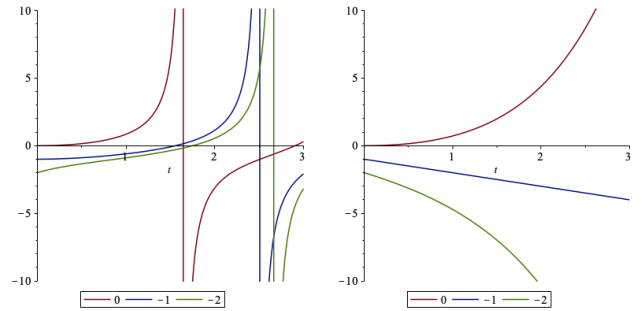


Figure 5: Illustration of Example 1. These two fields differ only by a constant translation. The algorithms are not objective because they are able to detect the DHTs in the left field but not in the right one.



(a) Trajectories of the input vector (b) Trajectories of the linearized vector field (29), DHT in blue.

Figure 6: Illustration of Example 2. Trajectories for different initial values show that neglecting the non-linear part lets the algorithm by Ide et al. return the blue line on the right, which is not a trajectory of the original field on the left.